energies

MDPI

Article

Strategies to Increase the Transient Active Power of Photovoltaic Units during Low Voltage Ride Through

Xiangwu Yan [1], Baixue Liang [1,*], Jiaoxin Jia [1], Waseem Aslam [2], Chenguang Wang [1], Shizheng Zhang [1] and Hongbin Ma [1]

[1] Key Laboratory of Distributed Energy Storage, Micro-Grid of Hebei Province, North China Electric Power University, No.619 Yonghua Road, Baoding 071003, China; xiangwuy@ncepu.edu.cn (X.Y.); jiajx33@163.com (J.J.); chenguang@ncepu.edu.cn (C.W.); shizheng@ncepu.edu.cn (S.Z.); hongbinm@ncepu.edu.cn (H.M.)

[2] Department of Electrical Engineering, University of Sargodha, Sargodha 40100, Pakistan; waseem.aslam@uos.edu.pk

* Correspondence: snowwhite@ncepu.edu.cn

Abstract: Due to a limitation in the magnitude of the three-phase output inverter currents, the output active power of the photovoltaic (PV) unit has been de-rated during low voltage ride through, which brings great instability risk to the power system. With the increase in the penetration rate of new energy, the impact of the power shortage on the system transient stability increases. It is of great significance to analyze the impact of this transient power shortage on system stability. This article explores methods to improve the active power output capability of photovoltaic units during low-breakthrough periods. A transient simulation model of a grid-connected PV generator with low-voltage ride-through (LVRT) capability is presented, under the condition of meeting the overcurrent capacity of the PV inverter and the requirement of dynamic reactive power support supplied by the PV generator specified in the China grid codes (GB/T 19964-2012) during grid fault. An example system with high PV penetration is built. The change principle and influencing factors of PV transient active power output are analyzed. The simulation model is designed in PowerFactory/DIgSILENT, and several types of three-phase voltage sags are performed in simulation to assess the impact of the active current reference calculation method and the maximum inverter output current (I_{max}) limit value on the PV active power output. According to the three indexes, namely the maximum active power of PV unit during the fault, the power improvement gradient and the power surge after the fault is cleared. Simulation results showed that using the orthogonal decomposition method to calculate the active current reference can make full use of the current capacity of the converter. Setting I_{max} to 1.1 rated current of photovoltaic inverter (I_N) can reduce the cost-effectiveness ratio of the transient active power output of the PV unit. Therefore, we aim to improve the unit's transient active power output capacity and realize the optimal effect of improving the transient active power shortage of the system.

Keywords: voltage sags; grid-connected photovoltaic system; low voltage ride through; transient active power

Citation: Yan, X.; Liang, B.; Jia, J.; Aslam, W.; Wang, C.; Zhang, S.; Ma, H. Strategies to Increase the Transient Active Power of Photovoltaic Units during Low Voltage Ride Through. *Energies* **2021**, *14*, 5236. https://doi.org/10.3390/en14175236

Academic Editor: Surender Reddy Salkuti

Received: 26 July 2021
Accepted: 13 August 2021
Published: 24 August 2021

1. Introduction

With the deterioration of the current environment and the exhaustion of traditional fossil energy, clean and efficient renewable energy, especially solar energy, has been used on a large scale. Photovoltaic (PV) generation has shown a large-scale grid-connection trend, with increasing installed capacity and an increasing penetration rate [1–5]. PV array needs to be converted from DC to AC by an inverter to access the grid, but the overcurrent capacity of the inverter is limited. When the grid suffers from fault, there may be transient overcurrent and overvoltage through the PV inverter. The instantaneous peak value will

exceed the maximum limit value of the inverter, which leads to the triggering of the PV system's overcurrent protection and the disconnection from the utility grid [6–9].

Therefore, in order to reduce the risk of PV systems going off the grid when the grid fails, and to improve the transient performance of the systems, these systems must remain connected to the grid within a certain voltage drop range and supply reactive power to support the grid, namely low-voltage ride-through (LVRT) capability [10]. If the PV array works at the maximum power point, the active power injected into the grid will be de-rated below the operating value no matter the DC bus voltage increases or decreases, which is conducive to the realization of low-voltage ride-through [11–13]. The national standard specifies the requirements for dynamic reactive power support capacity for the grid but does not specify the active power of PV units. During grid faults, the voltage of the PV parallel node decreases. The active power injected into the grid has been de-rated to avoid exceeding the inverter's capacity and assure injection of reactive power's priority for providing support to the grid voltage [14,15]. Thus, the active power shortage is inevitable in the system, affecting the system's transient stability. The Australian power grid accounts for 48.36% of new sources. Some new energy units are disconnected from the grid after extreme weather conditions because the present number of low-voltage ride-through (LVRT) is less than the number of failures, resulting in the continuous active power shortage of the system. At the same time, although some new energy units have successfully passed through the fault, they do not immediately recover to the output power level before the interference. It takes hundreds of milliseconds to recover, which leads to the transient active power shortage of new energy units. The active power shortage of these two parts makes the power flow of the line increase instantaneously, which leads to the overload of the tie line and the system jumping off, and the system becomes an isolated network operation and then collapses [16–18]. Therefore, it is important to study the transient active power changes during low-voltage ride-through and recovery of photovoltaic units in a high permeability system.

Scholars have done a lot of research on the LVRT of PV generation systems. In [3], the various possible fault current characteristics for solar photovoltaic generators considering low-voltage ride-through are established. However, this paper aims to discuss the performance of overcurrent relays, not the transient system stability. In [19], a study of a PV generator and its LVRT capability was carried out when voltage faults were introduced to the utility grid. However, this paper evaluates PV inverter behavior and influence on the grid regarding voltage support during grid fault. In light of the power grid current imbalance and power grid oscillation during low-voltage ride-through, a method for modeling and parameter optimization of grid-connected photovoltaic (PV) systems is proposed [20]. A new control strategy of active and reactive power is proposed to improve the reactive power support capability to provide a full range of voltage regulation for grid-connected PV systems during grid faults [21]. The article studies the control of PV inverters with the low-voltage ride-through capability to ensure the PV system remains connected during grid faults [14]. The improvement of the LVRT capability for a two-stage grid-connected inverter of a three-phase PV generator can be observed in [22]. The control of modular multilevel converters with LVRT capability is proposed [23]. However, as far as the authors are concerned, from decreasing transient active power shortage and improving system transient stability, the control strategies have not been commonly studied in the scientific literature. This paper will deal with this current lack of knowledge. Compared with the existing work, this paper's contribution includes:

(i) The characteristic and influence factors of active power supplied from the PV system in the fault are analyzed.

(ii) Under the premise of ensuring the safety of equipment overcurrent and meeting the reactive power support requirements in the Chinese grid, the PV inverter control strategies corresponding to different active current calculation formulas are established. The LVRT control block is added to the current and voltage loops in a grid-connected PV system's rotating orthonormal dq axes. The added LVRT control-block

regulates the reference for the quadrature q component of the output three-phase inverter currents (i_{q_ref}) according to the depth of the voltage sag, which attains an effective performance for reactive (Q) powers support during fault conditions. Meanwhile, the reference for the quadrature d component of the output three-phase inverter currents (i_{d_ref}) is regulated by different active current calculation formulas, obtaining different active power output.

(iii) A three-phase single-stage large power grid-connected PV system is analyzed and tested under several grid faults in PowerFactory/DIgSILENT. The influence of the d component of inverter currents (i_d) calculation formulas and the limitation of the inverter's output currents on the inverter's reactive power output is analyzed through simulation results.

The paper is organized as follows: Section 2 presents the LVRT capability of a PV system following the recommendations described in the Chinese grid codes (GB/T19964-2012). This section also describes the inverter control model. Section 3 presents the simulation results (using PowerFactory/DIgSILENT) of the system under investigation. The conclusion of the system performance is presented in Section 4.

2. Grid-Connected PV System Model with LVRT Capability

2.1. PV System Model

Figure 1 shows the block diagram of the three-phase single-stage grid-connected PV system presented in this article. The modeling of the PV power station mainly includes three parts: PV batteries, inverters and their control systems [24]. In Figure 1, p and q are the active and reactive power supplied to the grid, respectively. Us and δs are the amplitude and phase angle of the AC grid voltage, respectively. C_d and u_d are the DC capacitance and DC voltage, respectively. SPWM is the acronym of sinusoidal pulse width modulation. L is the abbreviation of filter inductance. u_{PV} is the operating voltage of the PV array. i_{PV} is the operating current of the PV array.

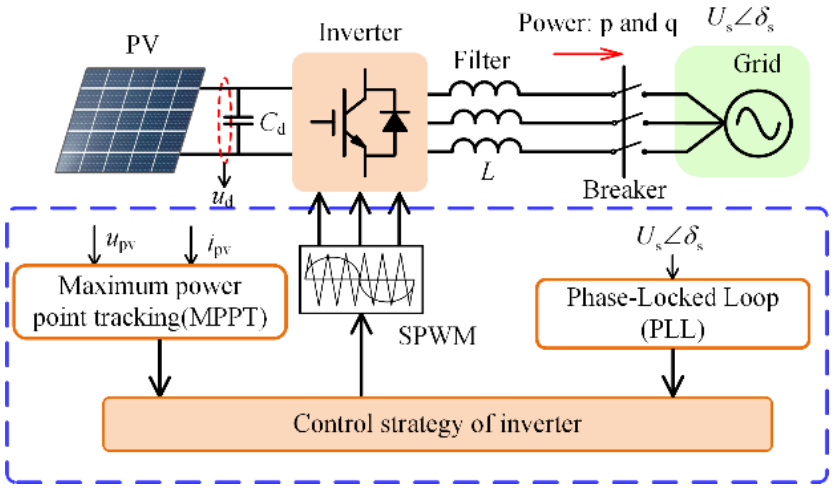

Figure 1. Structure of the proposed single-stage grid-connected PV system.

The PV generator does not have the same strong excitation function as a synchronous generator. During faulty operation of the grid, severe voltage fault happens. At the same time, the instantaneous active current has not changed, and thus the active power could not be delivered to the grid, which makes DC voltage increase. According to the PV curve for MPP, the operation point of PV array will shift from the maximum power point to the left side of the maximum power point. When the MPPT algorithm is deactivated, the active power injected into the grid can be calculated according to active current and grid voltage during the fault. It determines the active power delivered by the PV generator and adjust DC voltage to balance the active power, to realize the low-voltage ride-through [25].

2.2. Overall Control Model

The LVRT capability of a PV system requires the distributed generation (DG) systems to remain connected to the grid within a certain voltage sag and time interval during grid faults. The Chinese grid codes (GB/T19964-2012) are shown in Figure 2.

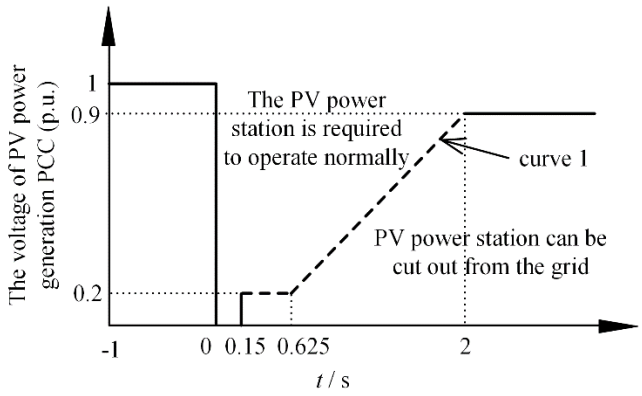

Figure 2. LVRT (low–voltage–ride–through) curves in Chinese grid code.

The PV generator delivers the maximum power to the utility grid during the normal operation. When the grid operates under faulty conditions, the DC voltage decreases and active power is de-rated below the operating value to achieve low-voltage ride-through. Thus, photovoltaic units can obtain LVRT capability by improving the inverter control strategy without additional hardware overhead. Its control goal is mainly to regulate the active (P) and reactive (Q) powers solely with the inverter currents' dq components to meet the requirements of the PV systems and provide dynamic reactive power support specified by the national standard. It also provides the limitation of the inverter currents to avoid its automatic disconnection from the utility grid, avoiding the inverter failure.

Figure 3 shows the control block diagram of PV inverter with LVRT capability presented in this paper [26]. During the normal operating conditions of the grid, a typical voltage and current double closed-loop inverter control strategy are adopted. As the conventional mode in Figure 3 displays, the outer voltage control loop tracks the DC side voltage, which corresponds to the maximum power and generates the active current reference as the active current command input of the current inner loop. Reactive current reference of the inner current control loop is set to zero in order to achieve a unity power factor to enhance the utilization factor of solar energy. During grid faults, to avoid the PV system's automatic disconnection from the utility grid, the PV inverter quits the conventional operation logic and enters the low-voltage ride-through operation logic, which is mainly divided into two modes, namely fault ride-through mode and recovery mode. From the moment the voltage of the PV grid-connected point drops to 90% of the normal value, the inverter enters the fault ride-through stage, adopting fault ride-through mode. The inverter control structure switches from the fault ride-through mode to the recovery mode when the voltage returns to 90% of the normal value, but the active power does not restore to normal levels immediately. The inverter switches back to the conventional mode when the active power climbs to the pre-fault level, as the fault ride-through mode and conventional mode in Figure 3 displays, respectively [27].

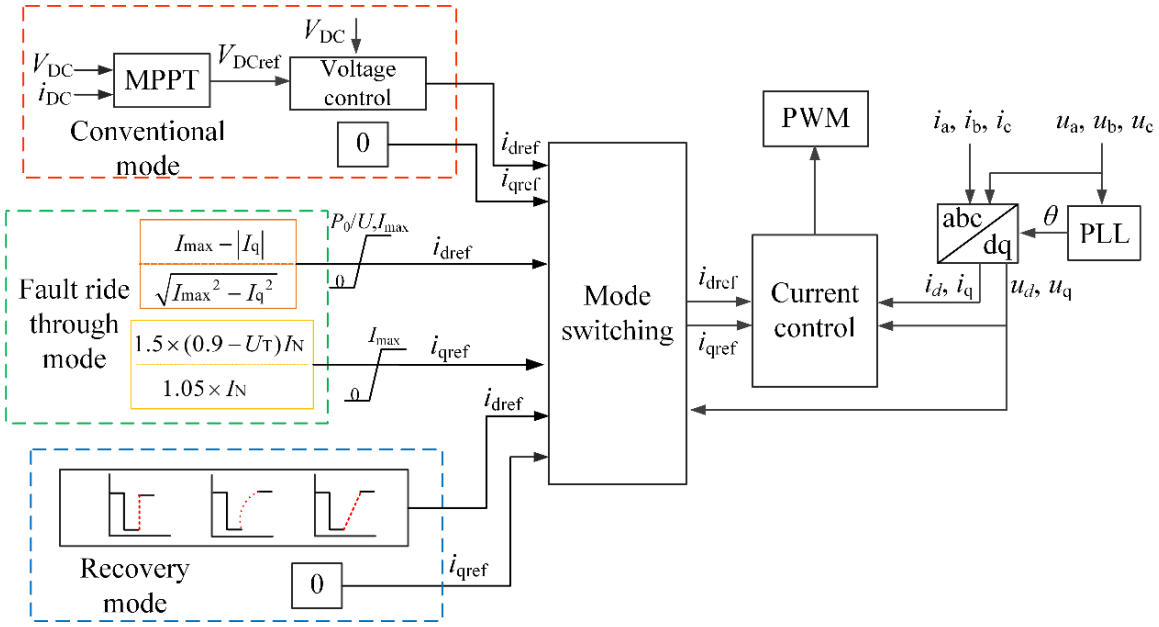

Figure 3. Control block diagram of PV inverter considering LVRT capability.

2.2.1. Inverter Reactive Current in Fault Ride-Through Mode and Recovery Mode

A reactive power priority strategy is adopted to supply reactive power for supporting the voltage recovery within the limit of the total current. Priority is given to regulate the reactive current output according to the depth of the voltage sag, and then the active current output of the inverter is regulated. No reactive current injection is required in the China grid codes as long as the grid voltage stays in the dead-band region (i.e., $0.9U_T \leq U_S \leq 1.1U_T$). On the other hand, if the grid voltage drops below 90% of the nominal value, reactive current injection is required (see Equation (1)).

$$I_q = \begin{cases} 1.5 \times (0.9 - U_T) I_N & (0.2 \leq U_T \leq 0.9) \\ 1.05 \times I_N & (U_T < 0.2) \\ 0 & (U_T > 0.9) \end{cases} \quad (1)$$

where I_N is the rated current of the inverter, and U_T is the grid voltage in per unit.

2.2.2. Inverter Active Current in Fault Ride-Through Mode and Recovery Mode

Figure 4 shows the inverter's active current during grid faults. The inverter active current decreases when grid voltage sags occur. During fault ride-through, there are two active current calculation formulas, namely using the error between the maximum allowable inverter current (I_{max}) and reactive current and applying the orthogonal decomposition method according to Equations (2) and (3). When the PV grid-connected point voltage recovers, but the inverter active power output does not yet recover to the pre-fault level (recovery stage), then the active current can be recovered in three ways: immediate recovery, specified slope rise or parabola rise [28]. The active current output of the photovoltaic unit cannot exceed the maximum allowable current (corresponding to the straight line y = I_{max} in Figure 4) and the maximum current that the PV array can provide (corresponding to the direct current of y = P_0/U_s in Figure 4).

$$I_d = \min\left(P_0/U_s, I_{max} - |I_q|\right) \quad (2)$$

$$I_d = \min\left(P_0/U_s, \sqrt{I_{max}^2 - I_q^2}\right) \quad (3)$$

where P_0 is the active power output before the fault; that is, the PV maximum active power output, and I_{max} is the allowable maximum inverter current.

It can be seen from Figure 4 that compared with the method of recovery active current rising according to the specified slope or parabola, the immediate recovery method can quickly restore the inverter active current output and thus attain the best performance for active powers support. Therefore, this paper focuses on regulating active current output by an immediate recovery in the recovery stage. P_0/U_s represents the maximum active current output supplied by PV array. Its value is substantial that the active current during the fault period will not exceed. Thus, the active current is mainly determined by the selected calculation formulas and I_{max} value under the same reactive current value.

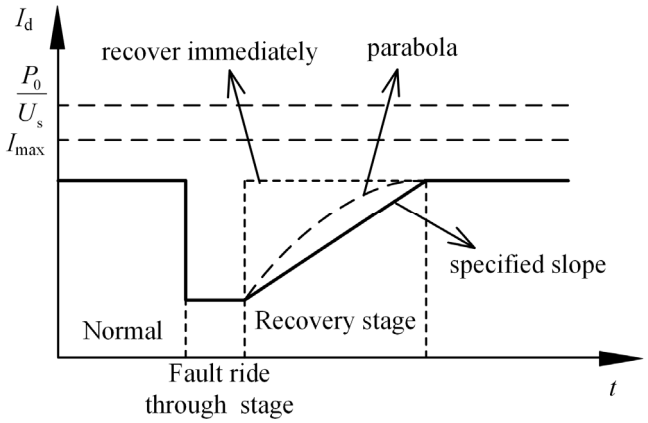

Figure 4. Transient active current response of PV unit with LVRT function.

2.3. Control of p and q

Based on the field-oriented vector control, the q components of the grid voltages are set to zero. According to the instantaneous power theory, the p and q powers delivered to the utility grid can be expressed as:

$$\begin{cases} p = \frac{3}{2} e_{\mathrm{d}} i_{\mathrm{d}} \\ q = \frac{3}{2} e_{\mathrm{d}} i_{\mathrm{q}} \end{cases} \quad (4)$$

where e_d is the d component of the grid voltage, and i_{dq} is the dq components of the inverter currents.

In conclusion, during grid faults, the amount of active power delivered by the inverter depends on the depth of the voltage sag, active current calculation formulas and the maximum allowable current. Because the fault type determines the depth of the system's voltage sag and fault location, it is impossible to control it in advance. Therefore, this paper focuses on the influence of active current calculation formulas and the maximum allowable current on PV units' transient active power characteristics.

3. Results and Discussion

Based on a standard 3-machine 9-node example system, a simulation model of a grid-connected PV generation system with high penetration (50%) is built upon the PowerFactory/DIgSILENT simulation platform, as shown in Figure 5. In order to keep the active power injected by each node in the original system unchanged, the synchronous generator (G2) is directly turned off, and the photovoltaic power station (PV) with the same output is used to replace it at the same location. The capacity and active power output during the normal operation of each generator in the system are shown in Table 1. The parameters of the established PV generator are listed in Table 2.

The simulation set up three-phase short-circuit faults at different locations. The fault occurred at 1 s. The duration of the fault was 150 ms, and the fault was cleared without disconnecting the line. As indicated in Figure 5, a three-phase short-circuit fault was

simulated in Bus7, Bus8 and A location. The corresponding voltage of PV parallel point was 1%, 30% and 50% of the normal value. In each fault scenario, the simulation was conducted with eight cases, as Table 3 displays.

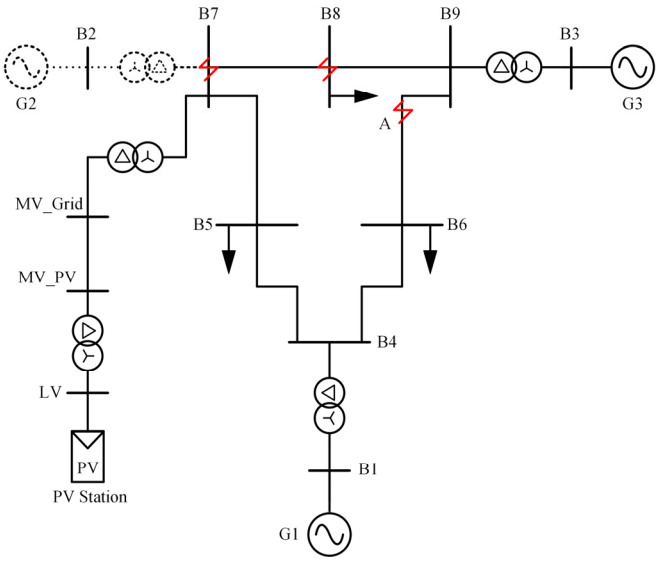

Figure 5. Simulink model of Power system with high PV penetration.

Table 1. The capacity and active power output of each power source during normal operation.

Generator	*P*(MW)	S_N (MVA)
G01	73.2	247.5
G02	163	192
G03	85	128
PV	163.1	182

The capacity of each generator (S_N), The active power output of each generator (P).

Table 2. Parameters of the established PV generator.

Parameter	Symbol	Value
Deadband for AC voltage support [p.u.]	deadband	0.1
Static for AC voltage support [-]	droop	1
MPP voltage of module in STC [V]	Umpp0	35
MPP current of module in STC [A]	Impp0	4.58
Initial DC voltage [V]	Udc0	700

Table 3. Working conditions corresponding to different types of three-phase short-circuit fault.

Fault Location	Working Condition	i_d Calculation Formula	I_{max} (I_N)
Line5/Bus7/Bus8	1	Equation (2)	1
	2		1.1
	3		1.2
	4		1.3
	5	Equation (3)	1
	6		1.1
	7		1.2
	8		1.3

As shown in Figure 6, the voltage sag of the PV parallel node is mainly determined by the fault location, having little effect on active currents. In combination with Figure 2, the PV system should remain connected to the grid during grid faults and supply reactive

power to support the grid in these 24 simulation scenarios. Take the fault at Bus8 as an example; increasing I_{max} can decrease the voltage surge at the moment of fault clearing, which smooths voltage recovery and reduces the impact on the grid. In this case, the total recovery time remains unchanged. When Bus7 or Line5 faults, it has the same rule.

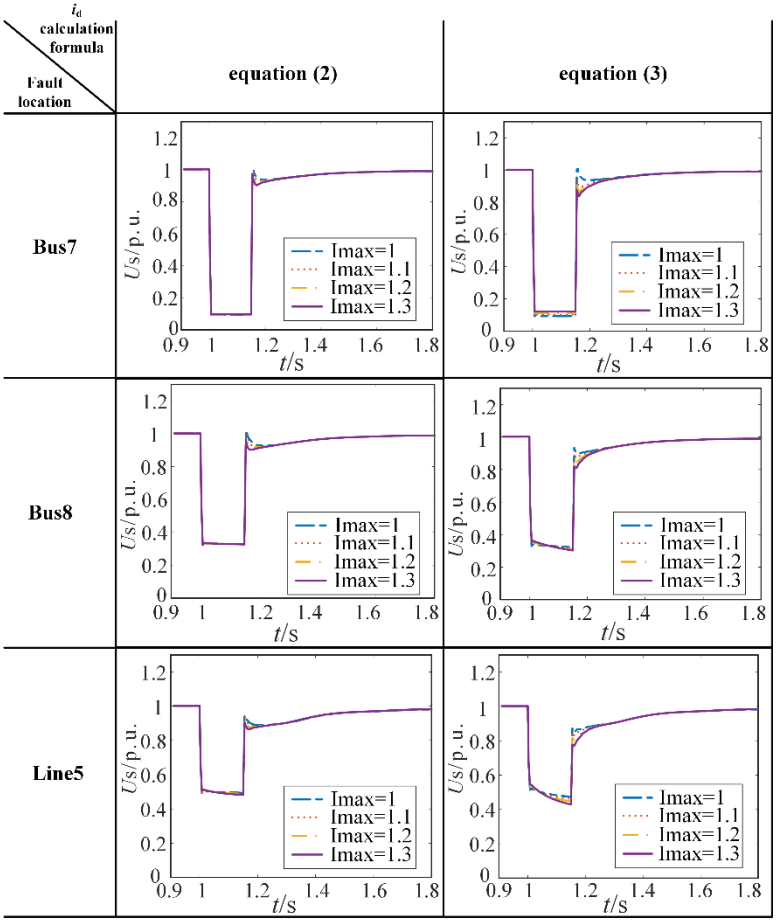

Figure 6. PV parallel node voltage in each simulation scenario.

3.1. Three-Phase Short-Circuit Fault on a Location

The results of the working condition (1) of the fault on location A are seen below in Figure 7.

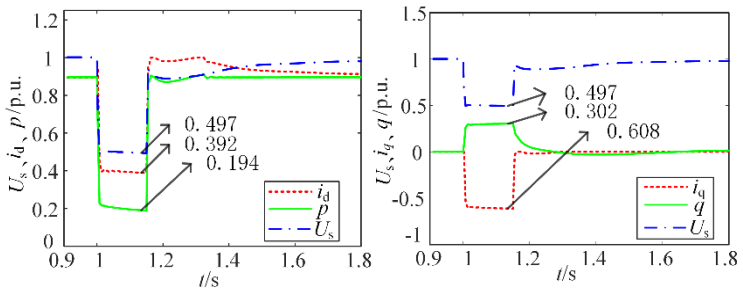

(**a**) (**b**)

Figure 7. Simulation results in case (1) of the fault on location A: (**a**) active output of PV generator; (**b**) reactive output of PV generator.

The voltage of the PV parallel node dropped to 0.497 p.u. at 1.11 s, which is around 0.199 kV (the base is 0.4 kV). Before and after the fault, both buses obtain values close

to nominal (1.002 p.u.). Considering these values, the following simple calculations can be performed:

$$dU_s = U_{sbeforefault} - U_{sdeaband} - U_{sduringthefault} = 1.002 - 0.1 - 0.497 = 0.405 \text{ p.u.} \quad (5)$$

The PV generator in a non-fault state supplies the LV bus with 0 p.u. reactive current, and since the droop parameter is 1.5 (Table 2) the reactive current injected from the PV generator (iq during the fault) is 0.608, which leads to

$$q_{duringthefault} = U_{sduringthefault} \cdot i_{qduringthefault} = 0.497 \times 0.608 = 0.302 \text{ p.u.} \quad (6)$$

According to the reactive current during a fault (0.608 p.u.) and the calculation Formula (2), it can be concluded that the active current during the fault is 0.392 p.u, which leads to

$$p_{duringthefault} = U_{sduringthefault} \cdot i_{ddurringthefault} = 0.497 \times 0.392 = 0.195 \text{ p.u.} \quad (7)$$

The above theoretical calculations are in accordance with simulation results shown in Figure 7, which indicates the effectiveness of the simulation model of the PV generator with LVRT capability and verifies the relationship between the transient active power, the voltage drop degree, the calculation method of the active current and the maximum allowable current of the inverter. The results of the other working conditions are the same.

The results of working conditions (1)–(8) when the fault occurs are shown below in Figures 8 and 9 and Table 4.

It can be seen from Figures 8 and 9, during grid faults, increasing I_{max} value can not only improve the active current but also have little influence on the voltage sag and thus reduce the active power shortage. However, the active current and active power increase sharply, accompanied by small-amplitude oscillation at the recovery stage. As shown in Figure 9, when I_{max} increases to 1.2, the active current during grid faults can be restored to the pre-fault level. However, because the voltage has not yet recovered, there is still a shortage of active power during the fault period.

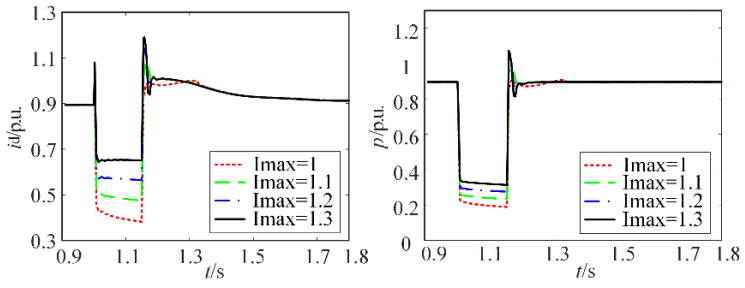

(**a**) (**b**)

Figure 8. Simulation results in cases (1)–(4) of the fault on location A: (**a**) active current; (**b**) active output.

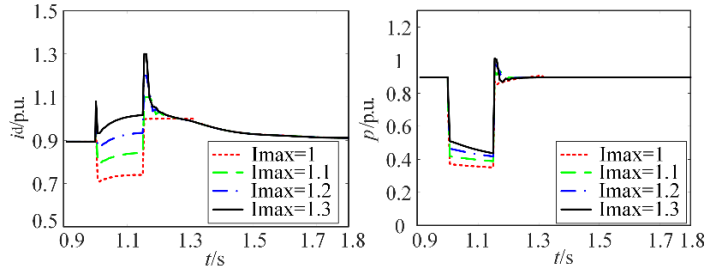

(**a**) (**b**)

Figure 9. Simulation results in cases (5)–(8) of the fault on location A: (**a**) active current; (**b**) active output.

Table 4. Active power index in cases (1)–(8) of the fault on location A.

Working Condition	$P_{\mathbf{frtmax}}$ (p.u.)	$\Delta p_{\mathbf{frt}}$ (p.u.)	$P_{\mathbf{rsmax}}$ (p.u.)
1	0.189	-	0.905
2	0.233	0.044	0.985
3	0.275	0.042	1.035
4	0.313	0.038	1.073
5	0.351	-	0.870
6	0.389	0.038	0.934
7	0.418	0.029	0.979
8	0.436	0.018	1.011

The maximum active power during the fault (P_{frtmax}), The increment of PV active power output corresponding to I_{max} increasing by 0.1 $I_{\mathbf{N}}$ (Δp), The power surge after the fault is cleared (P_{rsmax}).

It can be seen from the maximum power during the fault in Table 4, when Formula (3) is used to calculate the active current (corresponding cases 5–8), the PV active power output during the fault is greater than that of formula (2) (corresponding cases 1–4). Using Formula (3) to control the active current output during the fault can make greater use of the current capacity of the power conversion device and improve the active power shortage during the fault period. It can be seen from the power surge in Table 4, within the limits of the same value of I_{max}, applying the orthogonal decomposition method to calculate the active current (namely using Formula (3)) can reduce the active power surge after fault clearing and the impact on the power grid. It can be seen from the power improvement gradient in Table 4, when I_{max} is increased from 1 $I_{\mathbf{N}}$ to 1.1 $I_{\mathbf{N}}$, the improvement effect of active power during fault is the most significant. With the continuous rise in I_{max}, the active power improvement gradient becomes smaller; that is, the improvement effect on fault active power becomes smaller. The higher the limit value of the maximum output current of the inverter, the higher the cost is. The I_{max} is set to 1.1 $I_{\mathbf{N}}$.

Therefore, the simulation results of this fault condition verify that setting the maximum output current limit (Imax) of the photovoltaic inverter proposed in this paper as 1.1 I_{N}, and adjusting the active current output according to the orthogonal decomposition method during the fault period and the immediate recovery method during the recovery period, is the most effective control strategy.

3.2. Three-Phase Short-Circuit Fault of Bus8

The results of working conditions (1)–(8) of the three-phase short-circuit fault of Bus8 are seen below in Figures 10 and 11 and Table 5. The change rule is similar to the three-phase short circuit fault on location A. Using Formula (3) to control the active current output during the fault can make greater use of the current capacity of the inverter. Increasing I_{max} can improve the active current and reduce the active power shortage. It can be seen from Table 5 that with the increase in I_{max}, the degree of power improvement is decreasing. Comprehensively considering the improvement of active power and the increase of economic cost corresponding to the increase in I_{max}, I_{max} is still selected as 1.1 $I_{\mathbf{N}}$. Since the depth of voltage sag is greater than the three-phase short-circuit on location A, the PV output active power is less than the corresponding PV output active power at the three-phase short-circuit on location A.

The simulation results of this fault condition also verify that setting the maximum output current limit (I_{max}) of the photovoltaic inverter proposed in this paper as 1.1 I_{N}, and adjusting the active current output according to the orthogonal decomposition method during the fault period and the immediate recovery method during the recovery period is the most effective control strategy.

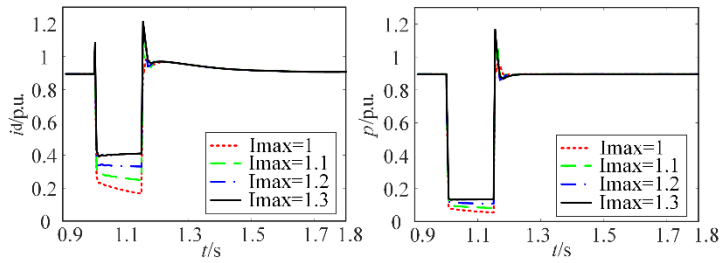

(**a**) (**b**)

Figure 10. Simulation results in cases (1)–(4) of the fault of Bus8: (**a**) active current; (**b**) active output.

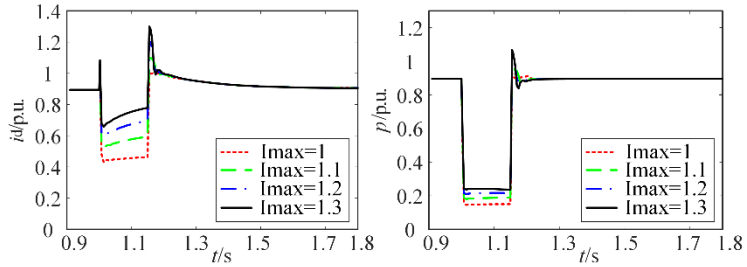

(**a**) (**b**)

Figure 11. Simulation results in cases (5)–(8) of the fault of Bus8: (**a**) active current; (**b**) active output.

Table 5. Active power index in cases (1)–(8) of the fault of Bus8.

Working Condition	$P_{\mathbf{frtmax}}$ (p.u.)	$\Delta p_{\mathbf{frt}}$ (p.u.)	$P_{\mathbf{rsmax}}$ (p.u.)
1	0.055	-	0.959
2	0.082	0.027	1.047
3	0.109	0.027	1.104
4	0.134	0.0025	1.166
5	0.145	-	0.928
6	0.180	0.035	0.988
7	0.210	0.030	1.035
8	0.236	0.026	1.068

The maximum active power during the fault (P_{frtmax}), The increment of PV active power output corresponding to $I_{\max}$ increasing by 0.1 $I_{\mathbf{N}}$ (Δp), The power surge after the fault is cleared (P_{rsmax}).

3.3. Three-Phase Short-Circuit Fault of Bus7

When three phase short circuit fault occurs in Bus7, the corresponding voltage drops to 1% of the normal value. Due to the severe voltage sag, any active power strategy hardly works, and the active power shortage is larger than that of the first two faults. The simulation results of working conditions (1)–(8) of the three-phase short-circuit fault of Bus7 are seen below in Figures 12 and 13. Different active current power strategies during the fault period have little difference in the effect of transient frequency stability, but during the recovery period, with the increase in $I_{\max}$, the fluctuation degree of active current and active power becomes larger.

Therefore, comprehensively considering the effects of different active current control strategies under the first two fault conditions, it can be concluded that the maximum output current limit of the photovoltaic inverter ($I_{\max}$) has been set to 1.1 I_{N} and the orthogonal decomposition method been used during the fault; the strategy of adjusting the active current output according to the immediate recovery method used during the recovery period can most effectively cope with various degrees of voltage drop faults in the system and improve the transient frequency stability of the system.

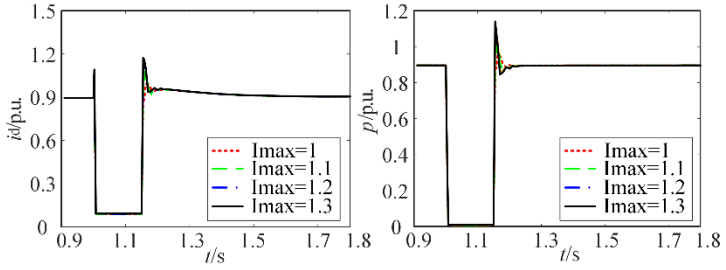

(**a**) (**b**)

Figure 12. Simulation results in cases (1)–(4) of the fault of Bus7: (**a**) active current; (**b**) active output.

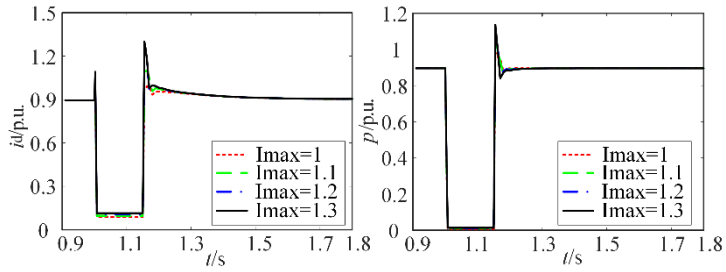

(**a**) (**b**)

Figure 13. Simulation results in cases (5)–(8) of the fault of Bus7: (**a**) active current; (**b**) active output.

4. Conclusions

In this article, a transient simulation model of a grid-connected photovoltaic (PV) generator with low-voltage ride-through (LVRT) capability is proposed. A power system model with a high PV penetration is established, and several types of three-phase voltage sags are simulated in PowerFactory/DIgSILENT. According to the three power indexes, namely the maximum active power of PV unit during the fault, the power improvement gradient and the power surge after the fault is cleared, the impact of the active current reference calculation method and the inverter allowable maximum inverter current (I_{max}) on the PV active power output is assessed. Additionally, methods to improve the active power output capability of photovoltaic units during low-breakthrough periods are explored. The conclusions are as follows:

(i) The active current control strategies have minimal effect on the voltage for grid-connected PV generation systems at the point of common coupling, so the PV transient active power has the same change in trend as the transient active current during grid fault. Effective performance for active power (P) support is attained by choosing the appropriate calculation method of active current and I_{max} value when voltage faults are introduced to the utility grid. It is carried out to meet the requirement of reactive powers (Q) support capability in China grid codes.

(ii) The error between the inverter current limitation (I_{max}) and reactive current is compared to obtain the active current values within the limits of the same value of I_{max}. Applying the orthogonal decomposition method to calculate the active current reference enhances the utilization factor of the inverter's capacity and increase the inverter active output current. It improves the active power shortage and boosts the transient stability of the power system.

(iii) Increasing I_{max} value can reduce the active power shortage during grid faults by increasing the active current output and improving the oscillation phenomenon in power recovery by reducing the excitation increment of active current and active power at the moment of fault clearing. However, increasing I_{max} value proportionally does not bring about an equal gradient of active power improvement effect, and the

cost becomes larger. Considering the economic cost and transient stability, the best way to regulate active current is to set I_{max} value as 1.1 I_N and apply the orthogonal decomposition method.

Author Contributions: Conceptualization, B.L., X.Y. and J.J.; methodology, B.L., X.Y. and J.J.; software, B.L. and J.J.; validation, B.L.; data curation, B.L.; writing—original draft preparation, B.L.; writing—review and editing, B.L., C.W., W.A., H.M., S.Z. and J.J. All authors have read and agreed to the published version of the manuscript.

Funding: This paper was supported by general projects of the Beijing Natural Science Foundation (3212037); Natural Science Funding of Hebei Province (E2018502134).

Acknowledgments: The authors gratefully thank the financial supports of the general projects of the Beijing Natural Science Foundation (3212037) and Natural Science Funding of Hebei Province (E2018502134). The authors of the article appreciate the referees for their valuable suggestions, which contributes to improving the paper.

Conflicts of Interest: The authors declare no conflict of interest.

References

1. Ludin, N.; Mustafa, N.; Hanafiah, M.; Ibrahim, M.A.; Teridi, M.A.M.; Sepeai, S.; Zaharim, A.; Sopian, K. Prospects of life cycle assessment of renewable energy from solar photovoltaic technologies: A review. *Renew. Sustain. Energy Rev.* **2018**, *96*, 11–28. [CrossRef]
2. Annapoorna, C.; Saha, K.; Mithulananthan, N. Harmonic impact of high penetration photovoltaic system on unbalanced distribution networks–learning from an urban photovoltaic network. *IET Renew. Power Gener.* **2016**, *10*, 485–494.
3. Oon, K.; Tan, C.; Bakar, A.H.A.; Che, H.; Mokhlis, H.; Illias, H. Establishment of fault current characteristics for solar photovoltaic generator considering low voltage ride through and reactive current injection requirement. *Renew. Sustain. Energy Rev.* **2018**, *92*, 478–488. [CrossRef]
4. Zhu, Y.; Kim, M.K.; Wen, H. Simulation and analysis of perturbation and observation-based self-adaptable step size maximum power point tracking strategy with low power loss for photovoltaics. *Energies* **2019**, *12*, 92. [CrossRef]
5. Benali, A.; Khiat, M.; Allaoui, T.; Denaï, M. Power quality improvement and low voltage ride through capability in hybrid wind-PV farms grid-connected using dynamic voltage restorer. *IEEE Access* **2018**, *6*, 68634–68648. [CrossRef]
6. Negnevitsky, M.; Nguyen, D.H.; Piekutowski, M. Risk assessment for power system operation planning with high wind power penetration. *IEEE Trans. Power Syst.* **2015**, *30*, 1359–1368. [CrossRef]
7. Hooshyar, H.; Baran, M.E. Fault analysis on distribution feeders with high penetration of PV systems. *IEEE Trans. Power Syst.* **2013**, *28*, 2890–2896. [CrossRef]
8. Bravo, R.J.; Yinger, R.; Robles, S.; Tamae, W. Solar PV inverter testing for model validation. In Proceedings of the IEEE Power Energy General Meeting, Detroit, MI, USA, 24–29 July 2011; pp. 1–7.
9. Mirhosseini, M.; Pou, J.; Agelidis, V.G. Single- and two-stage inverter-based grid-connected photovoltaic power plants with ride-through capability under grid faults. *IEEE Trans. Sustain. Energy* **2015**, *6*, 1150–1159. [CrossRef]
10. Wang, W.; Xv, W.; Liu, C. *Technical Requirements for Connecting Photovoltaic Power Station to Power System*; State Grid Corporation of China: Beijing, China, 2013.
11. Sangwongwanich, A.; Yang, Y.; Sera, D.; Soltani, H.; Blaabjerg, F. Analysis and modeling of interharmonics from grid-connected photovoltaic systems. *IEEE Trans. Power Electron.* **2018**, *33*, 8353–8364. [CrossRef]
12. Shang, L.; Zhu, W.; Li, P. Maximum power point tracking of PV system under partial shading conditions through flower pollination algorithm. *Prot. Control. Mod. Power Syst.* **2018**, *3*, 400–406. [CrossRef]
13. Zadeh, M.J.Z.; Fathi, S.H. A new approach for photovoltaic arrays modeling and maximum power point estimation in real operating conditions. *IEEE Trans. Ind. Electron.* **2017**, *64*, 9334–9343. [CrossRef]
14. Rey-Boué, A.B.; Guerrero-Rodríguez, N.F.; Stöckl, J.; Strasser, T.I. Modeling and design of the vector control for a three-phase single-stage grid-connected PV system with LVRT capability according to the Spanish grid code. *Energies* **2019**, *12*, 2899. [CrossRef]
15. Chen, Y.; Liu, J.; Zhou, J.; Li, J. Research on the control strategy of PV grid-connected inverter upon grid fault. In Proceedings of the International Conference on Electrical Machines and Systems (ICEMS), Busan, Korea, 26–29 October 2013; pp. 2163–2167.
16. Australian Energy Market Operator. *Preliminary Report—Black System Event in South Australia on 28 September 2016*; Australian Energy Market Operator Limited: Victoria Australia, 2016.
17. Australian Energy Market Operator. *Update Report—Black System Event in South Australia on 28 September 2016*; Australian Energy Market Operator Limited: Victoria Australia, 2016.
18. Australian Energy Market Operator. *Black System South Australia 28 September 2016—Third Preliminary Report*; Australian Energy Market Operator Limited: Victoria Australia, 2016.

19. Marinopoulos, A.; Papandrea, F.; Reza, M.; Norrga, S.; Spertino, F.; Napoli, R. Grid integration aspects of large solar PV installations: LVRT capability and reactive power/voltage support requirements. In Proceedings of the 2011 IEEE PES Trondheim PowerTech Power Technol, Trondheim, Norway, 19–23 June 2011.
20. Li, W.; Teng, Q.; Bin, Z.; Xiangjun, Z.; Qing, Y. Modeling and parameter optimization of grid-connected photovoltaic systems considering the low voltage ride-through control. *Energies* **2020**, *13*, 3972.
21. Jaalam, N.; Rahim, N.A.; Bakar, A.H.A.; Eid, B.M. Strategy to enhance the low-voltage ride-through in photovoltaic system during multi-mode transition. *Sol. Energy* **2017**, *153*, 744–754. [CrossRef]
22. Dehghani, T.H.; Maswood, A.I.; Konstantinou, G.; Pou, J.; Kandasamy, K.; Lim, Z.; Ooi, G.H.P. Low-voltage ride-thorough capability of photovoltaic grid-connected neutral-point-clamped inverters with active/reactive power injection. *IET Renew. Power Gener.* **2017**, *11*, 1182–1190. [CrossRef]
23. Rey-Boué, A.B.; Martinez-Rodrigo, F.; Guerrero-Rodríguez, N.F.; Lucas, H.L.C.; Pablo, S. Enhanced controller for grid-connected modular multilevel converters in distorted utility grids. *Electr. Power Syst. Res.* **2018**, *163*, 310–327. [CrossRef]
24. Theologitis, I.T. Comparison of Existing PV Models and Possible Integration under EU Grid Specifications. *Tek. Och Teknol.* **2011**. Available online: https://www.semanticscholar.org/paper/Comparison-of-existing-PV-models-and-possible-under-Theologitis/6f2d8648a795a831e1c6bd835a81f8946c29130a (accessed on 13 August 2021).
25. Zheng, F.; Ding, M.; Zhang, J. Modelling and simulation of grid-connected PV system in DIgSILENT/powerfactory. In Proceedings of the 2nd IET Renewable Power Generation Conference (RPG 2013), Beijing, China, 9–11 September 2013; pp. 1–6.
26. Zhu, L.; Ding, J.; Qu, L. *Guide for Modeling Photovoltaic Power System: GB/T32826—2016*; State Grid Corporation of China: Beijing, China, 2017.
27. Chao, P.; Li, W.; Peng, S.; Liang, X.; Xu, D.; Zhang, L.; Chen, N.; Sun, Y. A unified modeling method of photovoltaic generation systems under balanced and unbalanced voltage dips. *IEEE Trans. Sustain. Energy* **2019**, *10*, 1764–1774. [CrossRef]
28. Fan, S.; Chao, P.; Zhang, F. Modelling and simulation of the photovoltaic power station considering the LVRT and HVRT. *J. Eng.* **2017**, *13*, 1206–1209. [CrossRef]